

Implications of an Obscured AGN Model for the X-ray Background at Sub-mm and Far Infra-Red Wavelengths

Katherine F. Gunn^{*} and Tom Shanks

Department of Physics, University of Durham, South Road, Durham, DH1 3LE.

MNRAS - submitted.

ABSTRACT

Models invoking large populations of obscured AGN are known to provide good fits to the spectrum of the X-ray background and the observed soft and hard X-ray number counts. An important consequence of these models is that significant quantities of dust are required in order to provide the obscuring medium, which will be heated by the nuclear radiation from the AGN, and will radiate in the thermal infra-red. We therefore model the properties of the dust, and predict the contribution of obscured AGN to the intensity of the far infra-red background and the sub-mm source counts and redshift distribution, in order to ascertain whether our models are constrained further by the data available at these wavelengths. Our conservative models predict a contribution of between 5 and 15 per cent of the far infra-red background intensity, whereas if we use more extreme values for several parameters, this value may reach 33 per cent. This suggests that AGN may only form a significant minority of sub-mm sources, in agreement with the results of spectroscopic follow-up. Our models thus show that there is no inconsistency between obscured AGN models for the X-ray background and either sub-mm source counts or the intensity of the far infra-red background. We further propose that obscured AGN may explain the sub-mm emission associated with Extremely Red Objects (EROs). Finally, we make predictions for the redshift distribution of AGN sources detected in faint sub-mm surveys, which should allow future tests of this obscured AGN model.

Key words: diffuse radiation – X-rays: galaxies – galaxies: active – quasars: general

1 INTRODUCTION

Recently, enormous advances have been made in the field of sub-mm astronomy, most notably with the commissioning of SCUBA, the Sub-mm Common User Bolometer Array (Gear & Cunningham 1994; Holland et al. 1999), on the James Clark Maxwell Telescope (JCMT). The 850 μ m surveys of Smail, Ivison & Blain (1997), Hughes et al. (1998) and Barger et al. (1998) suggest that the sub-mm counts show strong evidence of evolution. The sources detected at this wavelength appear to be dusty, high redshift galaxies. However, the origin of the emission is not clear, and these distant dusty galaxies could be powered by either starburst or AGN activity. The question of which component dominates is highly important: if starbursts dominate, then it would imply that a significant amount of star-formation has been missed by studies which use ultra-violet techniques to claim that the star-formation rate (SFR) decreases in

galaxies at high redshift (Madau et al. 1996). Metcalfe et al. (1996) have previously suggested that models which include dust with a monotonically *increasing* SFR towards higher redshift can also give good fits to faint galaxy counts and colours (see also Wang 1991; Gronwall & Koo 1995; Campos & Shanks 1997; Steidel et al. 1999).

It has also been known for some time that some ultra-luminous infra-red galaxies (ULIRGs), which are strongly star-forming, dusty galaxies, also contain buried QSO nuclei. Images of ULIRGs in polarized light have shown highly anisotropic structure, such as that observed in the *IRAS* galaxy, F10214+4724, (Lawrence et al. 1993). Similar polarization structure is seen in Seyfert 2s and high redshift radio galaxies, which is thought to be indicative of non-uniform illumination consistent with the Unified Model of AGN. It has been inferred that the QSO and ULIRG phenomena are closely related, with ULIRGs being postulated as being Type 2 objects, or “QSO-2s” (Hines 1998). Genzel et al. (1998) have made *ISO* observations of ULIRGs in order to determine which is the dominant emission mechanism at FIR wavelengths. They find that ~ 75 per cent are powered

^{*} Present address: Department of Physics & Astronomy, University of Southampton, Highfield, Southampton, SO17 1BJ.

by star-formation, while the remaining ~ 25 per cent are AGN (see also Rigopoulou, Lawrence & Rowan-Robinson 1996). A massive dusty torus will also contain huge amounts of molecular gas, and therefore by definition will also be a prime site for star-formation. It has become increasingly evident that both AGN and starburst activity are often present in the same object, and therefore it is naïve to assume that the two processes are either independent or mutually exclusive.

The first spectroscopic follow-up of the faint sub-mm sources tends to show a mixture of dusty starburst and AGN. However, in obscured sources, it is frequently difficult spectroscopically to disentangle starburst from AGN components. Thus, in a SCUBA survey of four distant clusters of galaxies (Smail, Ivison & Blain 1997), the brightest source, SMM02399-0136, was found to be a hyperluminous, active galaxy at redshift $z = 2.8$ (Ivison et al. 1998). Frayer et al. (1998) compare the measured $L_{\text{FIR}}/L'_{\text{CO}}$ ratio of this high redshift galaxy, SMM02399-0136 (Ivison et al. 1998), to that of the local starburst, Arp 220, and find that it is twice as high. Since the FIR emission from Arp 220 is purely from merger-induced star-formation, they infer that approximately half of the FIR emission from SMM02399-0136 must therefore be due to a dust-enshrouded AGN. Further examples include the ultraluminous BALQSO, APM08279+5255, which at $z \sim 3.9$ is apparently the most luminous object currently known (Lewis et al. 1998), and the sub-mm source B1933+503, thought to be a high redshift ($z > 2$) dusty radio quasar (Chapman et al. 1999). Such surveys suggest that starburst galaxies dominate over AGN at faint sub-mm fluxes, but the area of sky and number of sources detected is still quite small.

Of course, large populations of such dust-enshrouded QSOs and AGN have been hypothesized in order to explain the observed shape of the X-ray background (XRB) spectrum (Madau, Ghisellini & Fabian 1994; Comastri et al. 1995; Gunn & Shanks 1999). In addition, the hard X-ray source counts are considerably higher than at soft X-ray energies (Georgantopoulos et al. 1997), implying the presence of an additional hard-spectrum population to the broad-line QSOs known to make up the bulk of the sources at lower energies. However, one of the central features of obscured QSO models is the presence of significant quantities of gas and dust surrounding the active nucleus, providing the means of absorbing a large fraction of the intrinsic radiation and affecting the observed properties in the optical and X-ray regimes. But this energy must escape somewhere, and through heating of the dust, the absorbed flux is re-radiated at far infra-red (FIR) wavelengths, providing an important test of the models. The amounts of dust invoked are quite considerable, and combined with the huge quantity of energy that must be radiated, plus the wide redshift distribution of these sources, would imply a substantial contribution to the FIR/sub-mm background radiation and source counts. This motivates our investigation here into the impact of obscured QSO models, used initially to explain observations at X-ray energies, at much longer wavelengths.

While this paper was in preparation, Almaini, Lawrence & Boyle (1999) have published sub-mm count predictions for obscured QSOs which give similar results to those described here. However, the conclusions of these authors are based on a simpler model where both the fit of the obscured QSOs to

the XRB and the obscured QSO sub-mm spectrum have to be assumed. We believe that the sub-mm predictions presented here are more robust since they are based on models which have been shown to give good fits to the X-ray background over its full energy range. In addition, in our method the absorption of the X-ray and optical spectra to produce the sub-mm spectra leaves no question as to their self-consistency.

In Section 2, we describe the latest measurements of the spectrum and intensity of the far infra-red background, and recent observations of the sub-mm source counts. Section 3 discusses how our obscured AGN model can be extended to these longer wavelengths, and describes how the emission from the obscuring dust torus has been modelled. The results are presented in Section 4, and are compared with the observed sub-mm number counts and the intensity of the far infra-red background at these wavelengths. We discuss the implications of our results in Section 5, and make predictions for the number-redshift relation for future $850\mu\text{m}$ surveys in Section 6.

Some of these results have already been discussed by Gunn (1999).

2 FAR INFRA-RED AND SUB-MM OBSERVATIONS

It is extremely difficult to measure the extragalactic far infra-red background (FIRB), due to the presence of foreground components from interplanetary zodiacal dust emission (peaking at $\sim 20\mu\text{m}$) and interstellar dust emission from our Galaxy (peaking at $\sim 150\mu\text{m}$). This zodiacal and galactic contamination must be carefully modelled, and subtracted to leave the extragalactic background. In addition, the cosmic microwave background (CMB) also contributes at these wavelengths, peaking at $\sim 1\text{mm}$, and this must also be accounted for. Once these components have been accurately modelled and removed, it should then be possible to detect any extragalactic FIRB.

The first detection of the FIRB was claimed by Puget et al. (1996), who used data from *FIRAS* on board *COBE*, taking advantage of the FIR window from $200 - 800\mu\text{m}$, between the peaks of the zodiacal emission and the CMB, and found that the intensity of the extragalactic background has the form:

$$\nu I_\nu \simeq 3.4 \left(\frac{\lambda}{400\mu\text{m}} \right)^{-3} \times 10^{-9} \text{ W m}^{-2} \text{ sr}^{-1},$$

in the range $400\mu\text{m} < \lambda < 1000\mu\text{m}$. More recent measurements have been made at shorter wavelengths using *DIRBE*, also on board *COBE* (Schlegel, Finkbeiner & Davis 1998; Hauser et al. 1998; Fixsen et al. 1998).

At longer wavelengths, there are several surveys currently in progress with the aim of resolving the source populations contributing to the sub-mm background. These surveys take advantage of the increased sensitivity and resolution now available with the SCUBA camera on the JCMT.

SCUBA sub-mm surveys can be divided into two types, the first being pointed observations of blank fields (Hughes et al. 1998; Barger et al. 1998; Eales et al. 1999). The second strategy is to make pointed observations of clusters of galaxies, in order to take advantage of the gravitational amplifica-

tion due to the lensing mass of the cluster (Smail, Ivison & Blain 1997). In this way, sources can be detected that would be fainter than the flux limit possible without the amplification factor, and in addition, due to the magnification of the source plane, there are fewer problems with source confusion. The $850\mu\text{m}$ number counts currently published can be fitted with a power-law of $N(> S) = 7.9 \times 10^3 S^{-1.1}$, where N is the number of sources per square degree detected above a flux limit of S mJy (Smail et al. 1998).

These recent measurements of both the spectrum of the far infra-red background, and the sub-mm number counts, now provide strict constraints with which to test theories of galaxy evolution, star-formation history, etc. In the SCUBA Lens Survey (Smail et al. 1998) sample of sub-mm sources, at least 20 per cent were found to show evidence for AGN activity (Barger et al. 1999). In the next Section, we investigate the implications of the obscured AGN hypothesis, by modelling their properties at sub-mm wavelengths. In Section 4, we predict the number of such sources expected from our models compared with the data described above, and put limits on their contribution to the far infra-red background.

3 MODELLING

Here we aim to use the obscured AGN models developed in Gunn & Shanks (1999) in order to make self-consistent predictions at sub-mm wavelengths. We assume that the luminosity absorbed at high energies is then reprocessed and emitted at lower energies, with a known thermal spectrum. The fluxes expected from such objects can then be estimated, from which we can predict sub-mm source counts and their contribution to the far infra-red background. The assumptions we have made are the following:

- The intrinsic $0.3 - 3.5$ keV X-ray luminosity of each source is known, and is assumed to come from the zero-redshift X-ray luminosity function, with parameters as described in Table 1.
- The column density, N_H , perceived by the optical, ultra-violet, and X-radiation is assumed to be a measure of the intrinsic amount of dust present, and is not affected significantly by the viewing angle. The covering factor, f_{cov} , of this obscuring material is defined to be the fraction of lines of sight for which a constant N_H is seen, and the remaining lines of sight are unobscured.
- All the absorbed flux goes into heating up the dust and gas in the obscuring medium, whatever the assumed geometry, which is then re-radiated isotropically in the thermal infra-red.

3.1 Column density distribution

Several different column density distributions have been proposed in order to explain the observed spectrum of the X-ray background. For example, Madau et al. (1994) used a bimodal model, consisting of a population of unabsorbed sources plus 2.5 times as many absorbed sources whose column densities had a Gaussian distribution with mean $\log(N_H/\text{cm}^{-2}) = 24.0 \pm 0.8$. Comastri et al. (1995) used

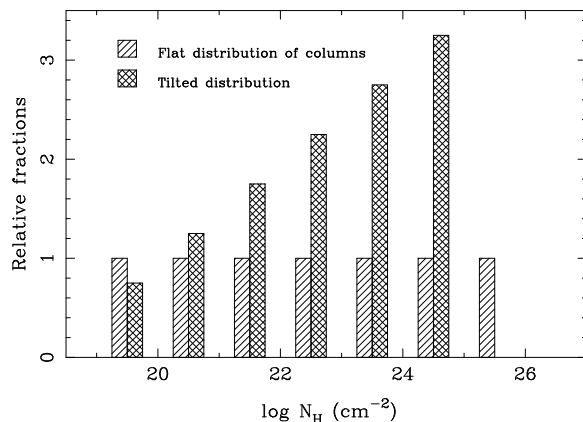


Figure 1. Comparison of the two distributions of obscured QSO populations used in this paper, where the size of each population is normalized relative to the unobscured $\log(N_H/\text{cm}^{-2}) \sim 19.5$ population. Our model of a flat distribution of columns is shown as hatched regions, and the tilted distribution is shown as cross-hatched regions, where the two models are shown slightly offset from one another for clarity. The tilted distribution has a greater proportion of high column density objects, as used to improve the fits to the data in a $q_0 = 0.5$ universe (Gunn & Shanks 1999).

four sub-classes of absorbed populations, each with a different normalization with respect to the unabsorbed population.

Here we use two models, the first being a *flat* distribution of columns, which was found in Gunn & Shanks (1999) to give good agreement with the observed X-ray source counts and XRB spectrum for a $q_0 = 0.0$ universe. The second model has a *tilted* distribution, with a greater proportion of high columns than in the flat model, which gives better agreement with the data in a $q_0 = 0.5$ universe. The differences in the observed properties of each population of sources are attributable solely to the column density. The *flat* distribution uses seven populations evenly spaced in log space: $\log(N_H/\text{cm}^{-2}) = 19.5, 20.5, 21.5, 22.5, 23.5, 24.5, 25.5$, each containing the same number and intrinsic luminosity function of AGN. The *tilted* distribution uses six populations, with the relative normalizations obeying the relation:

$$\Phi(N_H) = \left\{ 1 + 0.5 \log \left(\frac{N_H}{10^{20}} \right) \right\} \Phi^*.$$

The two distributions are compared in Fig. 1.

3.2 X-ray luminosity function and evolution

Since we are assuming that the observed sub-mm emission results from reprocessed nuclear X-ray and optical radiation, we take as a starting point a two power-law zero-redshift X-ray luminosity function (XLF):

$$\Phi_X(L_X) = \begin{cases} \Phi_X^* L_{X44}^{-\gamma_1} & L_X < L_X^*(z=0) \\ \Phi_X^* L_{X44}^{-\gamma_2} L_{X44}^{*(\gamma_2-\gamma_1)} & L_X > L_X^*(z=0), \end{cases}$$

where Φ^* is the normalization of the XLF, and L_{X44} is the $0.3 - 3.5$ keV X-ray luminosity in units of $10^{44} \text{ erg s}^{-1}$. Here the luminosity evolution is parametrized as either polynomial evolution:

$$L_X^*(z) = L_X^*(0) 10^{(\gamma_z z + \gamma'_z z^2)},$$

Table 1. Parameters of four Boyle et al. (1994) model fits to the *ROSAT* and *Einstein* EMSS QSO X-ray luminosity function and its evolution, as used in our calculations. The first column contains our adopted descriptive model name, POW(q_0) or POL(q_0), with the corresponding model name from Boyle et al. (1994) in the column headed B94. The XLF is parametrized by a broken power-law, with indices γ_1 and γ_2 below and above the break luminosity L_X^* . The evolution is described by either power-law or polynomial evolution, in both $q_0 = 0.0$ and $q_0 = 0.5$ universes.

Model	B94	q_0	Evolution	γ_1	γ_2	$\log L_X^*(0)^\dagger$	γ_z	z_{cut}	γ'_z	$\Phi_X^*\ddagger$
POW(0.0)	G	0.0	$(1+z)^{\gamma_2} + z_{cut}$	1.53	3.38	43.70	3.03	1.89		0.79
POW(0.5)	H	0.5	$(1+z)^{\gamma_2} + z_{cut}$	1.36	3.37	43.57	2.90	1.73		1.45
POL(0.0)	K	0.0	$\gamma_z z + \gamma'_z z^2$	1.50	3.35	43.71	1.14		-0.23	0.84
POL(0.5)	L	0.5	$\gamma_z z + \gamma'_z z^2$	1.26	3.32	43.52	1.15		-0.26	1.89

[†]where $L_X^*(0)$ is the 0.3 – 3.5 keV luminosity in units of erg s^{-1} .

[‡]where Φ_X^* is in units of $10^{-6} \text{ Mpc}^{-3} (10^{44} \text{ erg s}^{-1})^{-1}$.

or power-law evolution:

$$L_X^*(z) = L_X^*(0)(1+z)^{\gamma_2},$$

where a maximum redshift, z_{cut} , at which the evolution stops is incorporated, such that:

$$L_X^*(z) = L_X^*(z_{cut}) \quad z > z_{cut}.$$

The parameters for the XLF and its evolution have been taken from the fits to *ROSAT* and *Einstein* EMSS QSO number counts by Boyle et al. (1994), and are listed in Table 1. The broad line QSOs used to define the XLF correspond to our populations with $\log(N_H/\text{cm}^{-2}) = 19.5$ and 20.5, so we normalize the populations accordingly.

3.3 Canonical X-ray/optical QSO spectrum

The intrinsic QSO spectrum, $F(E)$, is assumed here to consist of two power-laws, with spectral indices $\alpha_x = 0.9$ (Nandra & Pounds 1994) and $\alpha_{opt} = 0.8$ (Francis 1993) at X-ray and optical energies respectively. In addition, the X-ray power-law is modified by the effects of reflection. The relative normalization is defined by a power-law of slope $\alpha_{ox} = 1.5$ joining 2 keV and 2500 Å (Tananbaum et al. 1979; Yuan et al. 1998). The behaviour of the spectrum between these two regimes is not well known however. Zheng et al. (1997) investigate the far ultra-violet properties of a sample of high redshift QSOs and find that the radio-quiet QSO spectrum can be approximated by a broken power-law, where the spectral break occurs at ~ 1050 Å (~ 0.01 keV). The spectral index at longer wavelengths is $\alpha_{opt} \sim 0.86 \pm 0.01$ (*c.f.* $\alpha_{opt} \sim 0.8$ used here), steepening significantly to shorter wavelengths (see also Laor et al. 1997). For simplicity, we therefore assume that the spectral break can be approximated by a step discontinuity at 0.01 keV.

3.4 Absorbed X-ray/optical QSO spectrum

The next step is to estimate the absorbed luminosity, L_{abs} , responsible for the heating of the torus, for each column density used. At X-ray energies, the opacity is dominated by photo-electric absorption at columns of $N_H < 10^{24} \text{ cm}^{-2}$. Above $N_H \sim 10^{24} \text{ cm}^{-2}$, the obscuring medium becomes Compton thick due to electron scattering, such that the effective optical depth is $\tau_{eff} = \tau_{ph} + \tau_{es}$. Since the absorbed fraction of the luminosity is almost unity above

$N_H \sim 10^{24} \text{ cm}^{-2}$ due to photo-electric absorption alone (see Fig. 2), we do not take electron scattering into account here as it does not affect our results significantly. The photo-electric absorption coefficients (Morrison & McCammon 1983) and can be evaluated using XSPEC (Arnaud 1996). In the optical, the dust extinction laws from Howarth (1983) and Seaton (1979) are used. A constant gas to dust ratio is implicitly assumed here. As the column increases, so does the amount of the continuum which is destroyed by these processes.

The absorbed luminosity can be approximated by calculating the energy at which the optical depth is unity for each process, $E(\tau_x = 1)$ and $E(\tau_{opt} = 1)$ respectively, as a function of the column density, and then by assuming that all the luminosity emitted between these two energies is absorbed. Using the relationship $\tau(E) = \sigma(E)N_H$, the cross-section scales as $\sigma(E) = 1/N_H$, for an optical depth of unity. The absorbed luminosity is then calculated from:

$$L_{abs} = f_{cov} \int_{E(\tau_{opt}=1)}^{E(\tau_x=1)} F(E) dE.$$

The range of intrinsic luminosities is defined by the X-ray luminosity function (XLF), so the absorbed luminosity is normalized by the known X-ray luminosity, L_X :

$$L_X = \int_{0.3 \text{ keV}}^{3.5 \text{ keV}} F(E) dE.$$

The fraction of the luminosity which is absorbed can then be calculated. Fig. 2 shows how the absorbed fraction increases with column density, saturating above $N_H \sim 10^{25} \text{ cm}^{-2}$, as no radiation whatsoever can escape unaffected from the nucleus, and all the emitted energy goes into heating up the obscuring medium.

3.5 Far infra-red QSO spectrum

Finally, we assume that all the absorbed radiation, L_{abs} , has to escape as thermal emission from the dust in the far infra-red, and therefore that $L_{FIR} = L_{abs}$. We also assume that the FIR luminosity is isotropic, and therefore that the received flux is independent of viewing angle. For the case for which the obscuring medium is also isotropic, this is a realistic assumption, as self-shielding of the inner regions means that only radiation from the outer, cooler layers of

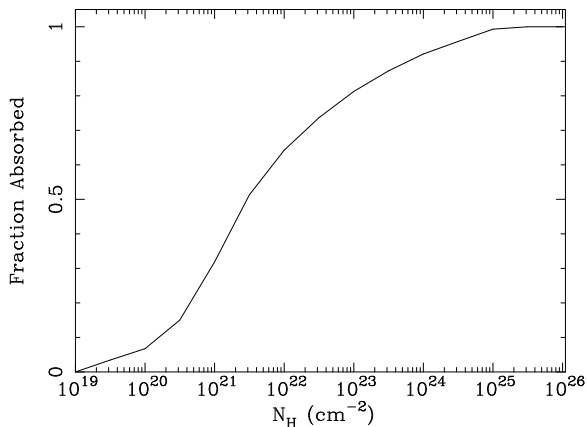


Figure 2. The fraction of the total X-ray and optical luminosity absorbed, as a function of the column density, N_H , for a covering factor of unity. Once the column is as high as $N_H \sim 10^{25} \text{ cm}^{-2}$, effectively all the energy is absorbed. For $f_{cov} = 0.5$, the fraction absorbed will be half that shown here.

dust will be received. However, for a toroidal geometry (e.g., $f_{cov} \sim 0.5$), radiation from the hot dust in the innermost regions will be able to escape from the top of the torus, and for face-on viewing angles, the spectrum will be broadened due to the superposition of components at a range of different dust temperatures (Pier & Krolik 1992). This has the effect of boosting the flux at short wavelengths ($\lesssim 10 \mu\text{m}$) but does not change the spectrum significantly at the wavelengths at which we are primarily concerned ($\gtrsim 100 \mu\text{m}$), as the hot emission component makes little contribution, and the torus is optically thick. As the true geometry is still unclear, neglecting this effect means that the predictions from our models at short wavelengths should be taken to be lower limits. We therefore choose to approximate our obscuring medium by isothermal dust, emitting isotropically.

By convention, at these energies, frequency units are used, and we write:

$$L_{\text{FIR}} = \int P(\nu_e) d\nu_e.$$

Assuming optically thin dust emission, the Planck function, $B(\nu, T)$, is modified by an opacity law, where the opacity depends on both the dust grain composition and the size and shape distribution of the grains, and which can be parametrized as $\kappa_d \propto \nu^\beta$. Following Cimatti et al. (1997), we use the opacity law:

$$\kappa_d = 0.15 \left(\frac{\nu_e}{250 \text{ GHz}} \right)^2 \text{ cm}^2 \text{ g}^{-1}.$$

The dust temperature is taken to be in the range $30 \text{ K} < T_d < 70 \text{ K}$ (Haas et al. 1998; Benford et al. 1998, 1999). Since the emitted FIR luminosity is constrained by the X-ray luminosity, the effect of increasing the assumed temperature means that the total normalization must be reduced in order to keep L_{FIR} constant, and vice versa.

The emitted power, $P(\nu_e)$, can therefore be parametrized as follows:

$$P(\nu_e) = 4\pi\kappa_d(\nu_e)B(\nu_e, T_d)M_d, \quad (1)$$

To calculate the received flux from such a source, we use the relationship:

$$S(\nu_o) d\nu_o = \frac{P(\nu_e)}{4\pi D_L^2} d\nu_e = (1+z) \frac{P(\nu_e)}{4\pi D_L^2} d\nu_o,$$

where D_L is the luminosity distance and $d\nu_e = (1+z) d\nu_o$, to give:

$$S(\nu_o) = \frac{(1+z)\kappa_d(\nu_e)B(\nu_e, T_d)M_d}{D_L^2}. \quad (2)$$

To calculate the integrated source counts as a function of flux density, we then use the same method as in Gunn & Shanks (1999), starting from the $0.3 - 3.5 \text{ keV}$ XLF, and using the above relationships between L_X and $S(\nu_o)$. Note that in the sub-mm regime, traditionally flux *density* is used, with units of Janskys, ($1 \text{ Jy} = 10^{-23} \text{ erg cm}^{-2} \text{ s}^{-1} \text{ Hz}^{-1}$), rather than the broad-band flux used at X-ray energies (units: $\text{erg cm}^{-2} \text{ s}^{-1}$), or optical magnitudes.

4 SUB-MM PREDICTIONS

Here we investigate the contribution to the sub-mm source counts and the far infra-red background predicted by our obscured AGN model. We look at the effects of changing certain parameters, such as the covering factor and temperature of the obscuring medium, the luminosity evolution of the AGN, and the maximum redshift at which these sources exist. At present, these parameters are not well constrained, particularly at high redshift. However, despite evidence that the space density of QSOs declines beyond $z \sim 3$ (Shaver et al. 1996), we know that QSOs exist at high redshift. New search techniques are discovering more such objects all the time, for instance the three QSOs found recently by the SDSS Collaboration (Fan et al. 1998), all with redshifts in the range $4.75 < z < 5.0$. As we are using luminosity functions and evolutionary models determined from X-ray selected QSOs, these have diverging properties above $z \sim 2$, and these can therefore be taken to span the range of likely properties. By invoking the most extreme cases, we are able to put firm upper limits on the obscured AGN contribution to both the source counts and FIRB intensity.

4.1 The covering factor of the absorbing material

In order to remain consistent with the assumed flat column distribution used in Gunn & Shanks (1999), we must also consider the covering factor of the obscuring material, as this affects the intrinsic distribution of column densities. Here, we take two examples, first that the obscuring material is isotropic, i.e., with a covering factor $f_{cov} = 1$, and secondly that a torus covers half the sky as perceived by the nucleus for all sources, i.e., $f_{cov} = 0.5$. We assume that these two values will span the true range of covering factors. Two intrinsic distributions giving rise to a *perceived* flat column distribution, as used in the $q_0 = 0.5$ model, are shown in Fig. 3.

A method for differentiating between these two proposed geometries for the obscuring material in AGN, is to determine the fraction which are highly luminous at sub-mm wavelengths. By definition, very little dust exists along the line-of sight to broad-line QSOs. Therefore, if the absorbing medium is isotropic, the dust content of broad-line QSOs must be intrinsically low, with low sub-mm emission.

Table 2. The contribution to the intensity of the FIRB at $850\mu\text{m}$ predicted by our obscured AGN model. The parameters used are as described in the text, where we have investigated the effects of changing the X-ray luminosity function and evolution, the covering factor of the obscuring medium f_{cov} and its temperature T_d , and the maximum redshift z_{max} . The predictions are compared with the observed $850\mu\text{m}$ background intensity from Fixsen et al. (1998) of $I_{\text{FIRB}} = 5.03 \times 10^{-10} \text{ W m}^{-2} \text{ sr}^{-1}$.

Model	f_{cov}	z_{max}	T_d (K)	I_Q ($10^{-11} \text{ W m}^{-2} \text{ sr}^{-1}$)	I_Q/I_{FIRB} (%)
POW(0.0)	1.0	5	30	8.70	17.4
POW(0.5)	1.0	5	30	3.80	7.6
POL(0.0)	1.0	5	30	5.41	10.8
POL(0.5)	1.0	5	30	2.23	4.5
POW(0.0)	0.5	5	30	6.85	13.2
POW(0.5)	0.5	5	30	3.00	6.0
POL(0.0)	0.5	5	30	4.08	8.2
POL(0.5)	0.5	5	30	1.75	3.5
POW(0.0)	1.0	2	30	1.30	2.6
POW(0.0)	1.0	10	30	16.4	32.9
POW(0.0)	1.0	5	50	1.04	2.1
POW(0.0)	1.0	5	70	0.149	0.3
POW(0.5)t	1.0	5	30	7.57	15.1
POL(0.0)t	1.0	5	30	4.45	8.9
POW(0.5)t	0.5	5	30	5.24	10.5
POL(0.0)t	0.5	5	30	3.05	6.1

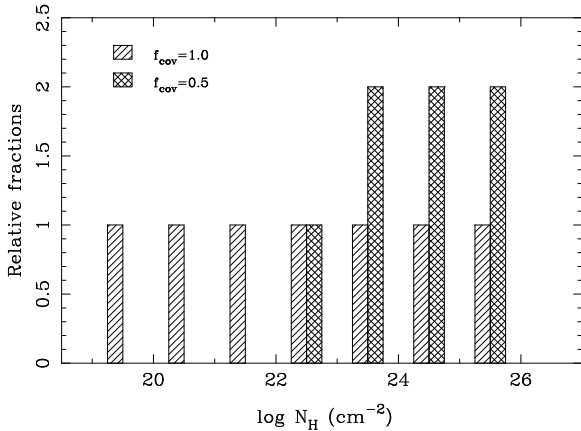


Figure 3. Comparisons of two different intrinsic column density distributions of obscured QSO populations, which give rise to the same *perceived* flat distribution, as used in the $q_0 = 0.5$ model. For an isotropic absorber, the covering factor is unity, i.e., $f_{cov} = 1$, and therefore an intrinsic flat distribution will also be perceived as flat (hatched regions); however, for an absorber for which $f_{cov} = 0.5$, a larger number of obscured sources are required, as half will be observed to be unobscured (cross-hatched regions); the two distributions are shown slightly offset from one another for clarity. For the tilted distribution of columns used in $q_0 = 0.5$ scenarios, a similar correction must be made when $f_{cov} = 0.5$ is assumed.

However, for a toroidal structure in the spirit of the Unified Model (Antonucci 1993), broad-line QSOs could contain large amounts of dust in a plane perpendicular to the line of sight. This is consistent with the large infra-red bump observed in the 3000 \AA to $300\mu\text{m}$ spectrum of a sample of Palomar Green QSOs (Sanders et al. 1989). Therefore, if all QSOs contain large quantities of dust, they will be strong sub-mm sources. Proposed sub-mm observations of X-ray

selected QSOs using SCUBA/JCMT will shed further light on this question in the near future.

4.2 The effects of changing the XLF parameters

We first investigate the predicted source counts for the obscured QSO model with a flat distribution of columns, integrated over redshifts $0 < z < 5$. The X-ray luminosity function used is evolved according to the power-law and polynomial models from Boyle et al. (1994), for both $q_0 = 0.0$ and $q_0 = 0.5$ cosmologies. The parameters of these models are detailed in Table 1.

First, we take as our fiducial model a power-law prescription for the luminosity evolution, and a $q_0 = 0.0$ cosmology, which we denote as POW(0.0). This model will be used hereafter, unless stated otherwise. In Fig. 4, we show the source counts predicted by this model, compared with the SCUBA data described in Section 2 and Fig. 4. A covering factor of $f_{cov} = 1$ is assumed, for a dust temperature of $T_d = 30 \text{ K}$, integrated over $0 < z < 5$. The contribution from each population of obscured QSOs is shown by a dashed line, with the total source counts denoted by a solid line. The reverse trend to that observed at X-ray energies is seen here: the populations with the smallest column densities give the lowest sub-mm fluxes, with the high column density populations dominating the sub-mm source counts due to the large dust masses present. This model predicts ~ 20 per cent of the source counts at 2 mJy , and flattens off at fainter fluxes, but will provide ~ 17 per cent of the FIRB at $850\mu\text{m}$.

In Fig. 5, the predictions for all four Boyle et al. models are shown, for covering factors of (a) $f_{cov} = 1$ and (b) $f_{cov} = 0.5$, using the intrinsic column distribution that each covering factor implies. As expected, the low q_0 models give a much larger contribution to the source counts than the $q_0 = 0.5$ models, due to volume effects. Taking the measured value for the $850\mu\text{m}$ FIRB intensity of

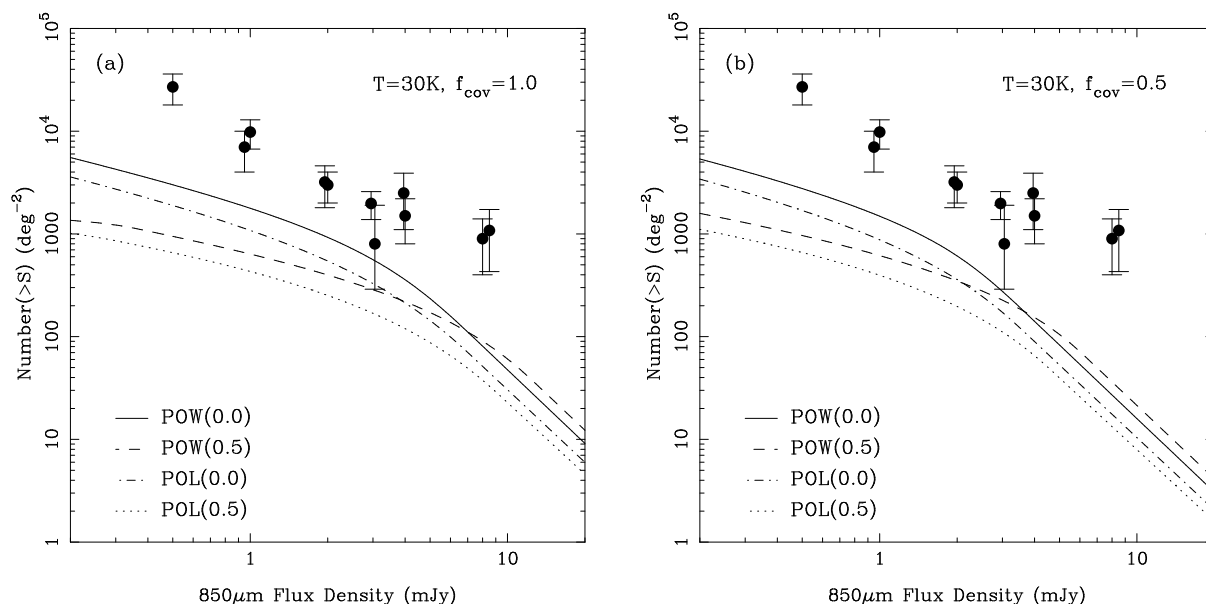


Figure 5. Total predicted $850\mu\text{m}$ source counts of obscured QSOs for models using power-law and polynomial evolution, $q_0 = 0.0$ and $q_0 = 0.5$ cosmologies, compared with the observed sub-mm counts as described in Fig. 4. A covering factor of (a) $f_{\text{cov}} = 1$, and (b) $f_{\text{cov}} = 0.5$, is assumed, with a dust temperature of $T_d = 30\text{ K}$, integrated over $0 < z < 5$. These models can account for between 17 per cent (POW(0.0), $f_{\text{cov}} = 1$) and 4 per cent (POL(0.5), $f_{\text{cov}} = 0.5$) of the FIRB. Note the change of scale with respect to Fig. 4.

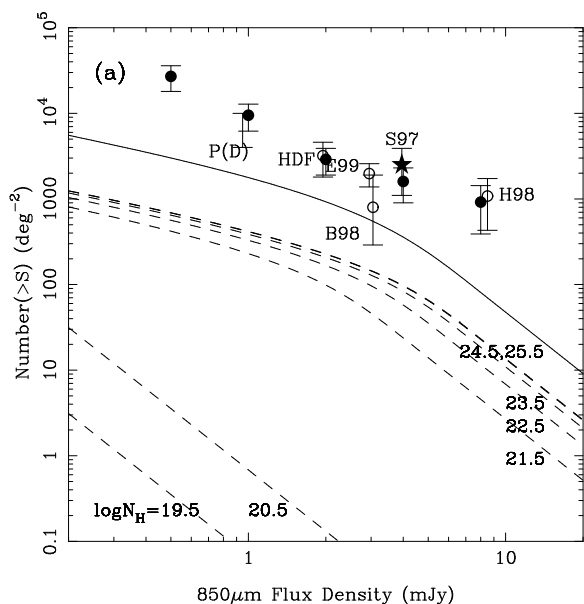


Figure 4. Predicted $850\mu\text{m}$ source counts of obscured QSOs, compared with the observed counts as described in Section 2. The filled circles show the results of the SCUBA Lens Survey (Blain et al. 1999), and the other points are as labelled: S97 - Smail, Ivison & Blain (1997); B98 - Barger et al. (1998); H98 - Holland et al. (1998); E99 - Eales et al. (1999); HDF, P(D) - Hughes et al. (1998). A dust temperature of $T_d = 30\text{ K}$ and a covering factor $f_{\text{cov}} = 1$ is assumed, integrated over $0 < z < 5$, for power-law luminosity evolution and $q_0 = 0.0$, model POW(0.0). The contribution from each individual population of obscured QSOs is shown as a separate dashed line, marked with the column density, and the total is shown by the solid line. In contrast to the X-ray number counts, here the biggest contribution comes from the most highly obscured objects, since these contain the largest amounts of dust. This model accounts for ~ 17 per cent of the FIRB.

$I_{\text{FIRB}} = 5.0 \times 10^{-10} \text{ W m}^{-2} \text{ sr}^{-1}$ from Fixsen et al. (1998), we calculate the fraction of the FIRB which can be accounted for by our obscured QSOs. Low q_0 models provide $\sim 8 - 17$ per cent of the FIRB intensity, compared with $\sim 3 - 8$ per cent for the $q_0 = 0.5$ models, as shown in Table 2.

The difference in the predicted number counts and background intensity between the $f_{\text{cov}} = 1$ and $f_{\text{cov}} = 0.5$ cases is due to the increased intrinsic far infra-red luminosity of sources which have an isotropic absorbing medium, as a greater fraction of the nuclear radiation is intercepted. These intrinsically brighter sources are therefore detected at higher fluxes, increasing the bright-end number counts. However, at faint fluxes, the predictions are similar for both assumed covering factors, implying that we are observing high redshift objects, which by definition will be the most luminous sources in either case.

For an isotropic covering medium, the predicted source counts of obscured AGN at 2 mJy account for between 8 and 20 per cent of the total counts, whereas for the anisotropic case, the numbers drop by about a third, since the objects are less luminous. The contribution to the intensity of the FIRB is $\sim 3 - 13$ per cent in the $f_{\text{cov}} = 0.5$ case, which is about 25 per cent lower than the $\sim 4 - 17$ per cent predicted for $f_{\text{cov}} = 1$.

4.3 The effects of changing z_{max} and T_d

If we were to assume that obscured QSOs exist out to redshift $z_{\text{max}} \sim 10$, then we can make a much larger contribution to the source counts and FIRB intensity, as shown for $T_d = 30\text{ K}$ and $f_{\text{cov}} = 1$ in Fig. 6(a). However, it is difficult to envisage a scenario in which large numbers of dusty QSOs form at such early epochs (Efstathiou & Rees 1988), and therefore this places a useful constraint on the

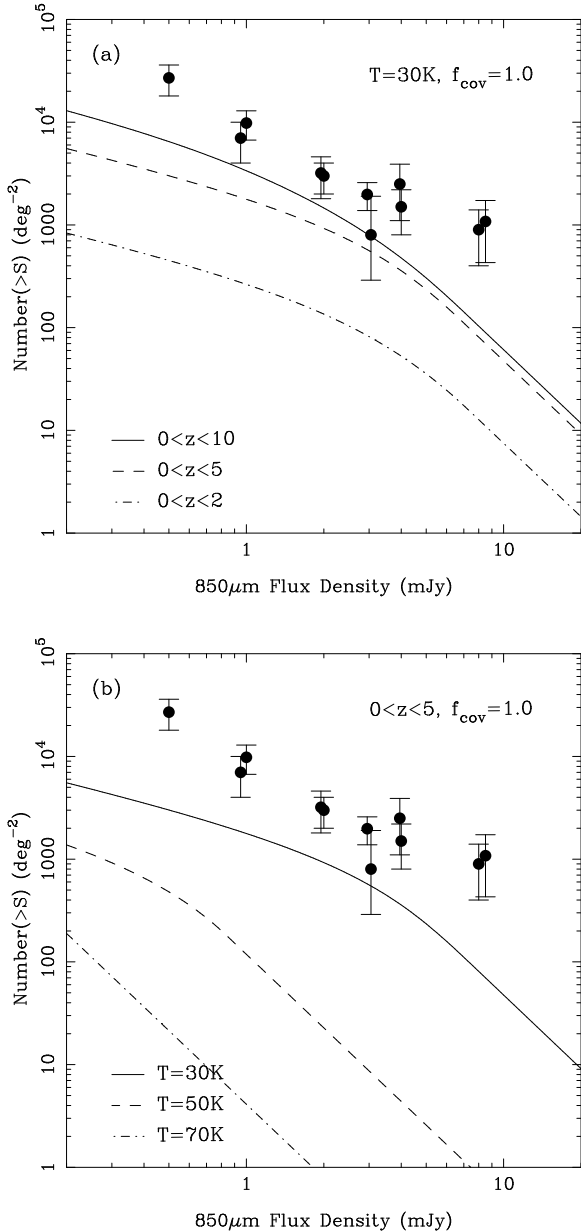


Figure 6. (a) The effect on the observed $850\mu\text{m}$ source counts, of varying the maximum redshift, z_{max} , for dust at $T_d = 30\text{ K}$, for $z_{max} = 2, 5$ and 10 . (b) The effect on the observed $850\mu\text{m}$ source counts, of varying the dust temperature between $T_d = 30\text{ K}$ and $T_d = 70\text{ K}$, over redshifts $0 < z < 5$. In both cases, parameters for our fiducial model POW(0.0) have been used, for seven populations with a flat column distribution, and a covering factor $f_{cov} = 1$.

maximum contribution such models can provide. Obscured QSOs from $0 < z < 10$ could contribute over 30 per cent of the Fixsen et al. (1998) measurement of I_{FIRB} .

There are very few complete sub-mm surveys of AGN at low and high redshifts in the literature, with enough data to constrain the dust temperatures in such objects. The uncertainties involved in making such estimates are high, where assumptions have to be made about the cosmology, the dust masses and the opacities, and in addition, observations at several different wavelengths are required in order to start

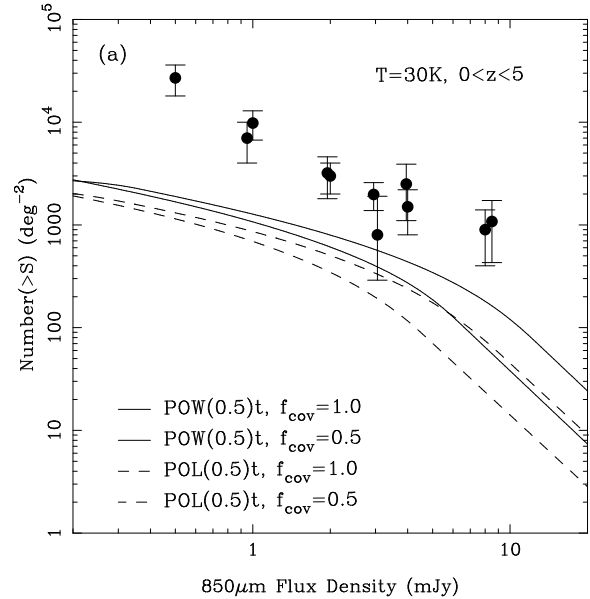


Figure 7. The predicted total source counts for the $q_0 = 0.5$ models, for power-law (solid lines) and polynomial (dashed lines) luminosity evolution, using a tilted distribution of column densities. Predictions for both a covering factor of $f_{cov} = 1$ (bold lines) and $f_{cov} = 0.5$ (thin lines) have been plotted, using $T_d = 30\text{ K}$ and $z_{max} = 5$.

to put limits on the parameters in the models. Treating the dust as isothermal is likely to be an oversimplification, but will be adequate for our purposes, and therefore we estimate that the range $30\text{ K} < T_d < 70\text{ K}$ should span the most probable temperatures.

For each column density used, the FIR luminosity is in effect fixed by the known amount of nuclear X-ray and optical luminosity which has been absorbed. If we increase the assumed dust temperature, the mass of the dust must be decreased in order to keep L_{FIR} constant. As the temperature is increased, the peak of the thermal radiation moves to higher frequencies, thereby reducing the intensity of the source at sub-mm energies. In Fig. 6(b), we show the effect of varying the temperature on the sub-mm counts, where the highest number of sub-mm sources are observed for the model with the lowest dust temperature. If the dust around most AGN is warm, $T_d \sim 70\text{ K}$, then the contribution to the $850\mu\text{m}$ FIRB will be negligible, whereas at $100\mu\text{m}$, their impact will be more significant.

4.4 Tilted column distributions for $q_0 = 0.5$ models

One further test here for the obscured QSO model is to look at the tilted distribution of column densities, which was invoked in order to obtain a better fit to the XRB for high density, $q_0 = 0.5$, models for the XLF. By skewing the distribution of objects towards higher column densities, this could have the effect of overpredicting the source counts and background intensity. However, in Fig. 7, it can be seen that the source counts predicted with this distribution for a range of models lie well below the observed counts, and flatten off towards fainter fluxes, again primarily due to volume effects. The maximum contribution to I_{FIRB} from these models is

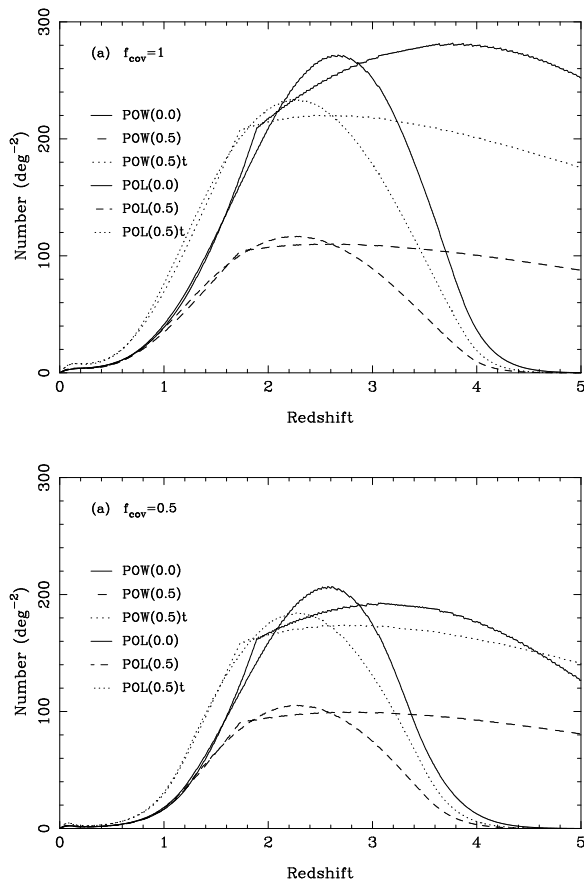


Figure 8. Predicted number-redshift distribution for an $850\mu\text{m}$ survey to 2mJy , of obscured QSOs with $T_d = 30\text{K}$, and $z_{max} = 5$, for covering factors of (a) $f_{cov} = 1$, and (b) $f_{cov} = 0.5$. Note the higher number densities predicted for low q_0 models.

~ 15 per cent, for model POW(0.5)t with $T_d = 30\text{K}$ and $f_{cov} = 1$.

4.5 Number-redshift distributions

In Fig. 8, we plot the number-redshift distributions predicted by our obscured QSO models, for an $850\mu\text{m}$ survey to 2mJy (*c.f.* the 1σ confusion limit for JCMT/SCUBA of 0.44mJy beam^{-1} ; Blain, Ivison & Smail 1998). Again, we use a dust temperature of $T_d = 30\text{K}$, and consider sources out to redshift $z_{max} = 5$, and make predictions for both (a) $f_{cov} = 1$ and (b) $f_{cov} = 0.5$. We have taken four models with a flat column distribution of seven populations of obscured AGN, and two models using a tilted distribution of six populations, as described in Section 3.1 (all for $f_{cov} = 0.5$). In the $q_0 = 0.0$ cosmology, the number of sub-mm sources predicted at redshifts $z > 3$ is much higher than for $q_0 = 0.5$, consistent with the steeper faint-end slope of the LogN:LogS relation for a low q_0 universe. Once more source identifications become available, it will be very straightforward to determine the form of the luminosity evolution, due to the fact that it is as easy to detect a sub-mm source at high redshift as at low redshift, and therefore if large numbers of high redshift obscured QSOs exist, they will be found in deep SCUBA surveys.

The follow-up identification programs for the latest

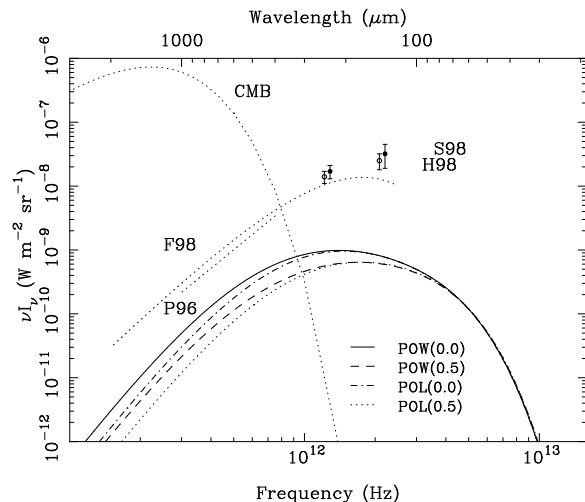


Figure 9. The predicted contribution to the FIRB from seven populations of obscured AGN with a flat column distribution, using power-law and polynomial luminosity evolution, for both $q_0 = 0.0$ and $q_0 = 0.5$ cosmologies, as labelled. A covering factor $f_{cov} = 1$ is used, with a dust temperature $T_d = 30\text{K}$, integrated over redshifts $0 < z < 5$. The data are as described in Section 2: CMB - Cosmic Microwave Background, Mather et al. (1994); F98 - Fixsen et al. (1998); P96 - Puget et al. (1996); H98 - Hauser et al. (1998); S98 - Schlegel et al. (1998).

SCUBA sub-mm surveys are nearing completion, and the source catalogues will soon be published. We shall therefore be able to compare the numbers of AGN detected with the redshift distributions predicted by our models. It is interesting to note that ~ 10 per cent of the optical counterparts to sub-mm sources are classified as Extremely Red Objects (EROs; Hu & Ridgway 1994), which are found in K -band images of the SCUBA error boxes (Smail et al. 1999). Deep radio maps provide more accurate positional information than the SCUBA maps, assuming that the radio and sub-mm emission is due to the same mechanism, and the ERO counterparts are confirmed by the radio data. It will be very difficult to obtain spectroscopic redshift information about these objects, even with a 10-m class telescope, as they are so faint in the optical, with $I \gg 25$. However, near infra-red spectroscopy has been used successfully to obtain a redshift of $z = 1.44$ for the ERO HR10 (Dey et al. 1999). Potentially, these could be examples of very highly obscured AGN at high redshift, for which in the optical and near infra-red we see the dusty host galaxy (hence the very red colours), and only see evidence for the AGN through the sub-mm and radio emission. Future deep surveys with AXAF and XMM, such as the proposed AXAF and SCUBA observations of the SSA 13 field (Cowie et al.), will provide a vital test of these theories, in searching for faint X-ray emission associated with these sources. However, unlike in the sub-mm regime, the X-ray k -correction is not working in our favour, and if we assume that these sources are at high redshift, then this is still an extremely ambitious project.

4.6 Predicted spectrum of the far infra-red/sub-mm background

We have shown from the sub-mm number counts predicted by our models that obscured AGN provide a small but non-negligible fraction of the intensity of the far infra-red background at $850\mu\text{m}$, ranging from 1 to 33 per cent. Fig. 9 shows the spectrum predicted from our flat distribution of column densities using a covering factor $f_{cov} = 1$, a dust temperature $T_d = 30\text{ K}$, and integrated over redshifts $0 < z < 5$. It can be seen that all four models predict the same intensity at high frequencies. This is to be expected, as the emission here is dominated by low redshift objects for which the rest-frame peak of the 30 K thermal spectrum is at $\sim 100\mu\text{m}$. Since the model parameters have been obtained from fits of the X-ray luminosity function to X-ray selected QSOs from *ROSAT* and the *Einstein* EMSS, which have relatively low median redshifts of $z \sim 1.5$ and $z \sim 0.2$ respectively, we would expect the predictions to diverge at high redshift and therefore low frequencies.

In Fig. 10, we show the effects of changing the maximum redshift and the dust temperature used in the models. In panel (a), it can be seen that the low redshift sources contribute at higher frequencies around $100\mu\text{m}$, whereas the high redshift sources account for the largest fraction of the FIRB intensity at $850\mu\text{m}$. In panel (b), we show how as the dust temperature is increased, the peak of the predicted FIRB background moves to higher energies. The integrated luminosity is fixed by the amount of absorbed nuclear X-ray and optical radiation, and is independent of temperature. Since this is a spectral energy distribution diagram, in which equal areas mean equal energies, then the predicted intensities for each model are identical after a shift along the frequency axis. A dust temperature of $T_d \sim 40\text{ K}$ would give the maximum contribution to the peak of the observed FIRB.

5 DISCUSSION

The first question to address is what these obscured AGN will look like at wavelengths other than the sub-mm. Compared with the majority of the X-ray source population, sub-mm sources have much higher dust masses and therefore much higher column densities. Hence in general, the optical and X-ray nuclear emission will be totally obscured, and the counterparts are likely to appear like relatively “normal” galaxies. These galaxies may perhaps have narrow emission lines in their optical spectra, possibly of high ionization species, or may look very dusty from their optical and infra-red colours. However, if the obscuring material is not assumed to be isotropic, then a fraction of these highly obscured sources will be orientated such that our line of sight lies within the opening angle of the torus, and therefore the X-ray and optical nuclear flux will escape unattenuated, while simultaneously a large sub-mm flux is detected from the dust in the torus.

The identification of optical counterparts to sub-mm sources has similar problems to those encountered with X-ray data, in that the point-spread function of the telescope is large (Half Power Beam Width = $14''.7$ at $850\mu\text{m}$ for SCUBA/JCMT), and therefore a number of plausible counterparts can lie in the error box. As sub-mm sources often

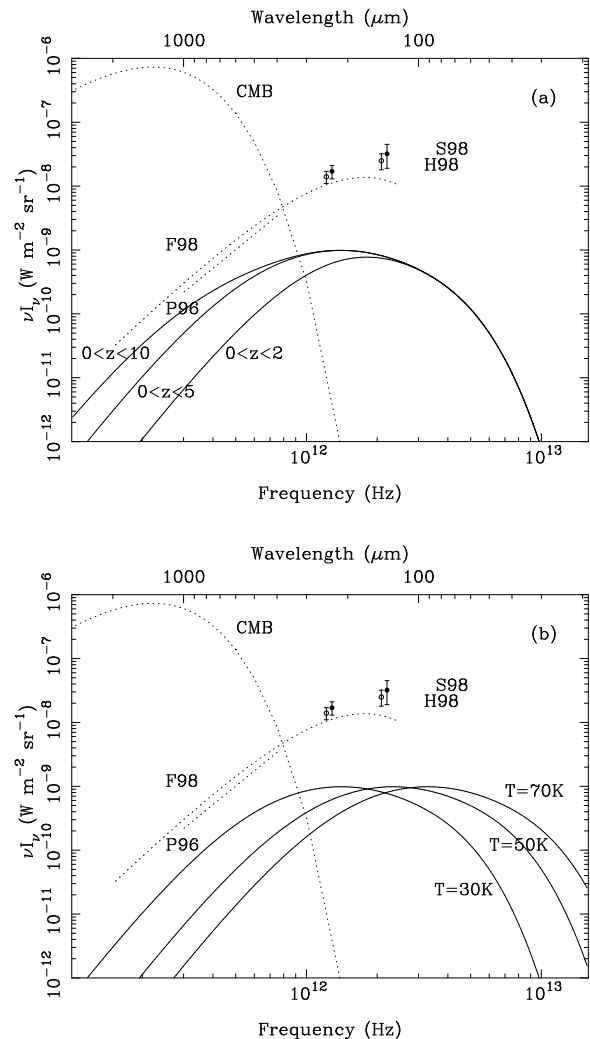


Figure 10. (a) The effect on the predicted FIRB spectrum of varying the maximum redshift, z_{max} , for dust at $T_d = 30\text{ K}$, for $z_{max} = 2, 5$ and 10 . (b) The effect on the predicted FIRB spectrum of varying the dust temperature between $T_d = 30\text{ K}$ and $T_d = 70\text{ K}$, over redshifts $0 < z < 5$. In both cases, our fiducial model has been used, for seven populations with a flat column distribution, and a covering factor $f_{cov} = 1$. The data are as described in Section 2.

have associated radio emission, deep radio maps of sub-mm survey fields have been taken (Ivison et al. in preparation; Richards 1998). Star-formation regions are expected to contain many supernova remnants, known to be strong radio emitters, and even radio-quiet AGN are likely to be detected as very faint, μJy sources in extremely deep radio maps. The high angular resolution of the radio data combined with the fact that radio emission is not affected by the presence of dust, means that optical counterparts to the sub-mm sources can be found in a much less ambiguous manner.

Once the counterpart has been found, the mechanism giving rise to the sub-mm emission must then be determined. By assuming that for starburst galaxies, the star-formation rate controls both the radio emission and the thermal sub-mm emission, Carilli & Yun (1999) use the radio to sub-mm spectral index as a redshift indicator. If however, an independent measure of the source redshift can be obtained,

then the radio to sub-mm spectral index can be used to infer whether there is any additional contribution to either component due to the presence of an AGN. A radio-loud AGN will have proportionally higher radio emission than a starburst galaxy, whereas an obscured radio-quiet AGN will have lower radio and higher sub-mm emission.

At present, there is little information available with which to constrain the dust temperature or range of temperatures that should be adopted for our models. Here, we have assumed that T_d remains constant with redshift, but as shown in Fig. 6, the temperature affects the predicted source counts significantly. The advent of larger samples of AGN at both low and high redshifts with multi-wavelength FIR/sub-mm data will enable any evolution of the dust temperature to be constrained.

Having chosen to keep T_d constant with redshift, and a universal opacity law, the only unconstrained parameter defining the luminosity is therefore the dust mass, M_d , (see Eqn 1). Therefore, since the FIR luminosity is directly related to the X-ray luminosity, which we have modelled to undergo pure luminosity evolution with redshift, then one possible interpretation is that the dust mass also evolves with redshift, with the form $M_d \propto (1+z)^3$. If the dust mass does not scale with the luminosity, then in order for our models to hold, there must be a balance between dust mass and temperature, with the mass compensating for changes in temperature.

A further consideration is the question of whether the assumption of constant gas to dust ratio at all redshifts is appropriate. For a QSO, there exists a radius within which the radiation field is so intense that dust particles will not survive, the so-called dust sublimation radius. Granato, Danese & Franceschini (1997) proposed that a significant quantity of gas exists inside the dust sublimation radius, and that a large proportion of the photo-electric absorption occurs within this region. This would have the effect of reducing the dust masses calculated using the column densities inferred from the observed photo-electric absorption at X-ray energies. This would in turn, lower the sub-mm fluxes from obscured AGN, cutting their contribution to the source counts and the intensity of the FIR background. However, the calculation of the gas to dust ratio for SMM 02399-0136 at redshift $z = 2.8$ by Frayer et al. (1998), and SMM 14011+0252 at redshift $z = 2.6$ by Frayer et al. (1999), from measurements of CO line emission combined with the sub-mm flux, gives a value similar to that found in nearby galaxies, from which they infer that CO emitting sources at high-redshift have already undergone significant chemical evolution. We have therefore chosen to adopt a constant gas to dust ratio in our models, since at present the available observations are insufficient to constrain any suitable alternatives.

6 FUTURE OBSERVATIONAL TESTS OF THE MODELS

The next decade promises to bring enormous advances in this field, with the advent of innovative instrumentation combined with the light-gathering capacity of 10-m class telescopes, plus the new generation of satellite-borne detectors. In the near infra-red, large area surveys will be possible with new wide-field cameras, such as the Cambridge Infra-

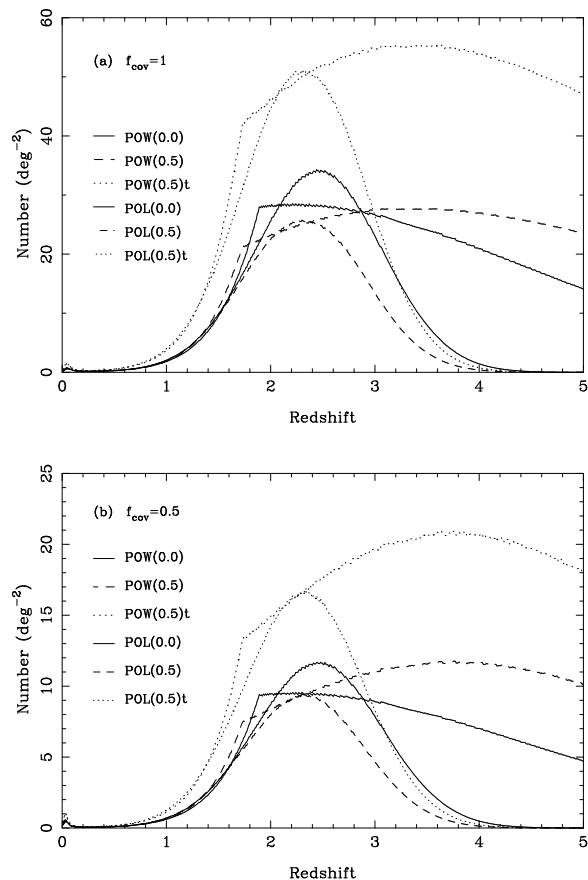


Figure 11. Predicted number-redshift distribution for an $850\mu\text{m}$ survey to 8 mJy , of obscured QSOs with $T_d = 30\text{ K}$, and $z_{max} = 5$, for (a) $f_{cov} = 1$ and (b) $f_{cov} = 0.5$. As in Fig. 8, we plot the $q_0 = 0$ models (solid lines) and $q_0 = 0.5$ models (dashed lines) for seven populations with a flat column distribution, and the tilted $q_0 = 0.5$ models with six populations (dotted lines). The power-law models are plotted with bold lines in each case, and the polynomial models are plotted with thin lines.

Red Survey Instrument (CIRSI; Beckett et al. 1997), allowing follow-up observations of the entire survey area for existing and future X-ray surveys, rather than the pointed observations of individual sources used previously. In the far infra-red, the FIRBACK survey (Lagache 1998) is an *ISOPHOT* $175\mu\text{m}$ survey of 4 deg^2 of sky at high Galactic latitudes, with the aim of determining the source populations making up the far infra-red background. Proposed satellite-borne mid and far infra-red observatories include the NASA *Space Infra-Red Telescope Facility (SIRTF; Werner 1998)*, and the ESA *Far Infra-Red and Sub-millimetre Telescope (FIRST; Pilbratt 1993; Genzel 1997)* scheduled for launch in 2001 and 2007 respectively.

In the sub-mm regime, a proposed wide area survey with SCUBA plans to cover a subset of the European Large Area *ISO* Survey region (ELAIS; Oliver et al. 1998) of around 640 square arcminutes (0.178 deg^2). The survey will have a brighter flux limit than existing deep pencil-beam surveys, and aims for a 3σ detection threshold of $\sim 8\text{ mJy}$, from which ~ 40 sources are expected. Our predictions for the number-redshift distribution for such a survey are presented in Fig. 11(a) for $f_{cov} = 1$, with the more conservative

predictions using $f_{cov} = 0.5$ in Fig. 11(b). The expected number of sources ranges between $\sim 14 \text{ deg}^{-2}$ (POL(0.5), $f_{cov} = 0.5$, $z_{max} = 5$) and $\sim 180 \text{ deg}^{-2}$ (POW(0.5)t, $f_{cov} = 1$, $z_{max} = 5$), depending on the evolution and column density distribution used in the model. Clearly, if the obscuring torus is also a site of active star-formation and the sub-mm flux of each component is comparable (Frayer et al. 1998), then the number of AGN may be somewhat higher than predicted on the basis of the above model.

7 CONCLUSIONS

In this paper, we have extended the obscured QSO model for the X-ray background of Gunn & Shanks (1999) to the sub-millimetre regime, by considering the fate of the X-ray, ultra-violet and optical energy absorbed by the obscuring medium. This energy goes into heating up the dust in the obscuring material, which then radiates thermally at far infra-red and sub-millimetre wavelengths. We have modelled the obscuring medium as either isotropic or having a toroidal geometry, which then dictates the intrinsic column density distributions which are consistent with the line-of-sight distributions found from X-ray and optical observations.

Since the spectrum in the sub-mm is rising steeply to higher frequencies, the k -correction obtained is such that our obscured QSOs are equally visible for redshifts of $1 < z < 10$. We therefore use the observed sub-mm source counts at $850 \mu\text{m}$ and the spectrum of the far infra-red background to constrain our models, by ensuring that the large quantities of cool dust invoked would not exceed the observed emission.

We have shown that a variety of plausible obscured AGN models, which provide good fits to the X-ray background spectrum and the number counts at soft and hard X-ray energies, are consistent with the observed sub-mm source counts and intensity of the FIRB. The models predict between 1 and 33 per cent of the FIRB intensity, and a similar fraction of the number counts, depending on how extreme is the model, but with the more conservative models predicting between 5 and 15 per cent. This is in good agreement with the fact that the majority of sub-mm sources are identified as starburst galaxies, providing the complementary sources. In addition, the obscured AGN models may be a suitable candidate for the source of the sub-mm emission associated with EROs.

Finally, we have made predictions of the redshift distribution of sub-mm sources from our models, for both existing and proposed surveys, and described how combined X-ray and sub-mm survey data will be able to determine the extent of the obscured QSO contribution to cosmological backgrounds at both high and low energies.

ACKNOWLEDGMENTS

This paper was prepared using the facilities of the STAR-LINK node at Durham. KFG acknowledges receipt of a PPARC studentship. We thank Chris Done and Ian Smail for useful discussions.

REFERENCES

- Almaini O., Lawrence A., Boyle B. J., 1999, MNRAS, 305, L59
 Antonucci R., 1993, ARA&A, 31, 473
 Arnaud K. A., 1996, in Jacoby G.H., Barnes J., eds, *Proc. of the ADASS V Conference*: ASP Conf. Series 101: San Francisco, Vol. 5, p. 17
 Barger A. J., Cowie L. L., Sanders D. B., Fulton E., Taniguchi Y., Sato Y., Kawara K., Okuda H., 1998, Nat, 394, 248
 Barger A. J., Cowie L. L., Smail I., Ivison R. J., Blain A. W., Kneib J. P., 1999, AJ, 117, 2656
 Beckett M. G., Mackay C. D., McMahan R. G., Parry I. R., Piche F., Ellis R. S., 1997, SPIE Proc., 2871, 1152
 Benford D. J., Cox P., Omont A., Phillips T. G., 1998, AAS Meeting, 192, 1104
 Benford D. J., Cox P., Omont A., Phillips T. G., McMahon R. G., 1999, ApJL, 518, L65
 Blain A. W., Ivison R. J., Smail I., 1998, MNRAS, 296, L29
 Blain A. W., Kneib J. P., Ivison R. J., Smail I., 1999, ApJL, 512, L87
 Boyle B. J., Shanks T., Georgantopoulos I., Stewart G. C., Griffiths R. E., 1994, MNRAS, 271, 639
 Campos A., Shanks T., 1997, MNRAS, 291, 383
 Carilli C. L., Yun M. S., 1999, ApJL, 513, L13
 Chapman S. C., Scott D., Lewis G. F., Borys C., Fahlman G. G., 1999, MNRAS submitted. (astro-ph/9810444)
 Cimatti A., Bianchi S., Ferrara A., Giovanardi C., 1997, MNRAS, 290, L43
 Comastri A., Setti G., Zamorani G., Hasinger G., 1995, A&A, 296, 1
 Dey A., Graham J. R., Ivison R. J., Smail I., Wright G. S., Liu M., 1999, ApJ, 519, 610
 Eales S., Lilly S., Gear W., Dunne L., Bond J. R., Hammer F., Le Fevre O., Crampton D., 1999, ApJ, 515, 518
 Efstathiou G., Rees M. J., 1988, MNRAS, 230, 5P
 Fan X., Strauss M., SDSS Collaboration, 1998, *SDSS Press Release*
 Fixsen D. J., Dwek E., Mather J. C., Bennett C. L., Shafer R. A., 1998, ApJ, 508, 123
 Francis P. J., 1993, ApJ, 407, 519
 Frayer D. T. et al., 1999, ApJL, 514, L13
 Frayer D. T., Ivison R. J., Scoville N. Z., Yun M. S., Evans A. S., Smail I., Blain A. W., Kneib J. P., 1998, ApJL, 506, L7
 Gear W. K., Cunningham C. R., 1994, SPIE Proc., 2198, 613
 Genzel R., 1997, in ASP Conf. Series 124: *Diffuse Infrared Radiation and the IRTS*, San Fransisco, p. 465
 Genzel R. et al., 1998, ApJ, 498, 579
 Georgantopoulos I., Stewart G. C., Blair A. J., Shanks T., Griffiths R. E., Boyle B. J., Almaini O., Roche N., 1997, MNRAS, 291, 203
 Granato G. L., Danese L., Franceschini A., 1997, ApJ, 486, 147
 Gronwall C., Koo D. C., 1995, ApJL, 440, L1
 Gunn K. F., 1999, PhD Thesis, University of Durham.
 Gunn K. F., Shanks T., 1999, MNRAS submitted.
 Haas M., Chini R., Meisenheimer K., Stickel M., Lemke D., Klaas U., Kreysser E., 1998, ApJL, 503, L109
 Hauser M. G. et al., 1998, ApJ, 508, 25
 Hines D. C., 1998, American Astronomical Society Meeting, 193, 2704
 Holland W. S. et al., 1999, MNRAS, 303, 659
 Howarth I. D., 1983, MNRAS, 203, 301
 Hu E. M., Ridgway S. E., 1994, AJ, 107, 1303
 Hughes D. H. et al., 1998, Nat, 394, 241
 Ivison R. J., Smail I., Blain A. W., Kneib J. P., 1999, in preparation.
 Ivison R. J., Smail I., Le Borgne J. F., Blain A. W., Kneib J. P., Bezecourt J., Kerr T. H., Davies J. K., 1998, MNRAS, 298, 583

- Lagache G., 1998, in *Wide Field Surveys in Cosmology*, 14th IAP meeting, Editions Frontieres, p. 301
- Laor A., Fiore F., Elvis M., Wilkes B. J., McDowell J. C., 1997, *ApJ*, 477, 93
- Lawrence A. et al., 1993, *MNRAS*, 260, 28
- Lewis G. F., Chapman S. C., Iбата R. A., Irwin M. J., Totten E. J., 1998, *ApJL*, 505, L1
- Madau P., Ferguson H. C., Dickinson M. E., Giavalisco M., Steidel C. C., Fruchter A., 1996, *MNRAS*, 283, 1388
- Madau P., Ghisellini G., Fabian A., 1994, *MNRAS*, 270, L17
- Mather J. C. et al., 1994, *ApJ*, 420, 439
- Metcalfe N., Shanks T., Campos A., Fong R., Gardner J. P., 1996, *Nat*, 383, 236
- Morrison R., McCammon D., 1983, *ApJ*, 270, 119
- Nandra K., Pounds K. A., 1994, *MNRAS*, 268, 405
- Oliver S. et al., 1998, in *Wide Field Surveys in Cosmology*, 14th IAP meeting, Editions Frontieres, p. 165
- Pier E. A., Krolik J. H., 1992, *ApJ*, 401, 99
- Pilbratt G., 1993, *Advances in Space Research*, 13, 912
- Puget J. L., Abergel A., Bernard J. P., Boulanger F., Burton W. B., Desert F. X., Hartmann D., 1996, *A&A*, 308, L5
- Richards E. A., 1999, *ApJL*, 513, L9
- Rigopoulou D., Lawrence A., Rowan-Robinson M., 1996, *MNRAS*, 278, 1049
- Sanders D. B., Phinney E. S., Neugebauer G., Soifer B. T., Matthews K., 1989, *ApJ*, 347, 29
- Schlegel D. J., Finkbeiner D. P., Davis M., 1998, *ApJ*, 500, 525
- Seaton M. J., 1979, *MNRAS*, 187, 73P
- Shaver P. A., Wall J. V., Kellermann K. I., Jackson C. A., Hawkins M. R. S., 1996, *Nat*, 384, 439
- Smail I., Ivison R. J., Blain A. W., 1997, *ApJL*, 490, L5
- Smail I., Ivison R. J., Blain A. W., Kneib J. P., 1998, in *After the dark ages: when galaxies were young (the Universe at $2 < z < 5$)*. (astro-ph/9810281)
- Smail I., Ivison R. J., Kneib J. P., Cowie L. L., Blain A. W., Barger A. J., Owen F. N., Morrison G., 1999, *MNRAS* in press. (astro-ph/9905246)
- Steidel C. C., Adelberger K. L., Giavalisco M., Dickinson M., Pettini M., 1999, *ApJ*, 519, 1
- Tananbaum H. et al., 1979, *ApJL*, 234, L9
- Wang B., 1991, *ApJL*, 383, L37
- Werner M. W., 1998, American Astronomical Society Meeting, 193, 2502
- Yuan W., Brinkmann W., Siebert J., Voges W., 1998, *A&A*, 330, 108
- Zheng W., Kriss G. A., Telfer R. C., Grimes J. P., Davidsen A. F., 1997, *ApJ*, 475, 469